Biomedical Signal Processing and Control 18 (2015) 1–10

Contents lists available at ScienceDirect

Biomedical Signal Processing and Control

journal homepage: www.elsevier.com/locate/bspc

Technical Note

# Wavelet and fast bilateral filter based de-speckling method for medical ultrasound images

Ju Zhang [a], Guangkuo Lin [a], Lili Wu [a], Chen Wang [a], Yun Cheng [b,*]

[a] College of Information Engineering, Zhejiang University of Technology, Hangzhou 310023, China
[b] Department of Ultrasound, Zhejiang Hospital, Hangzhou 310013, China

ARTICLE INFO

*Article history:*
Received 10 July 2014
Received in revised form
28 November 2014
Accepted 29 November 2014
Available online 29 December 2014

*Keywords:*
Wavelet
Fast bilateral filter
Medical ultrasound image
Speckle noise

ABSTRACT

Speckle noise is an undesirable part of the ultrasound imaging process, since it can degrade the quality of ultrasound images and restrict the development of automatic diagnostic techniques for ultrasound images. Aiming at the problem of speckle noise, an improved de-speckling method for medical ultrasound images is proposed, which is based on the wavelet transformation and fast bilateral filter. According to the statistical properties of medical ultrasound image in the wavelet domain, an improved wavelet threshold function based on the universal wavelet threshold function is considered. The wavelet coefficients of noise-free signal and speckle noise are modeled as generalized Laplace distribution and Gaussian distribution, respectively. The Bayesian maximum a posteriori estimation is applied to obtain a new wavelet shrinkage algorithm. High-pass component speckle noise in the wavelet domain of ultrasound images is suppressed by the new shrinkage algorithm. Additionally, the coefficients of the low frequency signal in the wavelet domain are filtered by the fast bilateral filter, since the low-pass component of ultrasound images also contains some speckle noise. Compared with other de-speckling methods, experiments show that the proposed method has improved de-speckling performance for medical ultrasound images. It not only has better reduction performance than other methods but also can preserve image details such as the edge of lesions.



## 1. Introduction

Ultrasonic imaging, CT, MRI and other imaging techniques have been widely used in clinical diagnosis. Ultrasound imaging technology is safer than other imaging techniques because it is non-invasive, non-radioactive, convenient and efficient. Therefore, the clinical application of ultrasonic imaging technology has become more important, especially in observing the growth status of the fetus in pregnant women and diagnosis of lesions of the abdominal organs.

However, the existence of speckle noise has degraded the quality of ultrasound images and restricted the development of automatic diagnostic techniques, especially for ultrasound breast imaging. Every year about 500,000 women die from breast cancer partially due to the lack of clear breast ultrasound images. Speckle noise is an undesirable part of the ultrasound image, which masks the small difference in gray level and degrades the image quality. Speckle noise results from a random scattering phenomenon in imaging cell resolution. Therefore, de-speckling is an important step before the analysis and processing of ultrasound images, and many researchers are attracted to devote their efforts to this issue.

According to principles of ultrasonic imaging, the ultrasonic envelope signal received by the ultrasonic imaging system is modeled as a multiplicative model of signal and noise, where the multiplicative noise is speckle noise. On the basis of signal-to-noise ratio (SNR), multiplicative noise in the spatial domain can be modeled by Rayleigh distribution [1], Rician distribution [2], *K* distribution [3], etc. In order to improve terminal display on most ultrasonic imaging instruments, the ultrasonic envelope signal is compressed with logarithmic transformation. After the logarithmic transformation, an improved medical ultrasonic image remains. Additionally, after the logarithmic transformation, the multiplicative noise model is converted to an additive noise model, where the noise can be simplified as Gaussian white noise. Then the 2-D discrete wavelet transformation (DWT) is applied for the log-transformed image. Because wavelet transformation is a linear transform processing, the noise coefficients in the wavelet domain

* Corresponding author. Tel.: +86 13221807158.
*E-mail addresses:* zjk@zjut.edu.cn (J. Zhang), chengyun.zjhospital@gmail.com (Y. Cheng).

http://dx.doi.org/10.1016/j.bspc.2014.11.010
1746-8094/

are modeled by zero-mean Gaussian distribution and wavelet coefficients of the log-transformed noise-free ultrasound image are modeled by generalized Laplacian distribution [4].

In recent decades, several image filtering techniques had been proposed to reduce speckle noise. These de-speckling filters are classified into five categories [5]: local adaptive filters, anisotropic diffusion filters, multi-scale filters, nonlocal means filters and hybrid filters. Commonly used adaptive filters (Lee [6], Frost [7] and SRBF [8]) assume that speckle noise is essentially multiplicative noise. Anisotropic diffusion filters include DPAD [9], SUSAN_AD [10] and OSRAD [11]. Nonlocal means filters are novel de-noising algorithms, such as OBNLM [5], PPB [12] and Guo [13]. For multi-scale filters (wavelet soft/hard threshold's filter [14] and Andria [15]), the wavelet transformation is usually used as a tool to analyze and process the image. Hybrid filters are the combination of several methods. For example, the SAR-BM3-D's filter [16] is the combination of a multi-scale filter with a nonlocal means filter. Wavelet theory has been widely used in image processing due to the advantages of time–frequency analysis and multi-scale analysis. The wavelet de-noising method is better than others in the processing of additive noise, and this method has higher efficiency, which can satisfy general product demand. However, using the wavelet transformation de-noising method to suppress speckle noise of medical ultrasonic images usually cannot get desirable results, because the low-pass component also contains some speckle noise.

In this paper, a novel de-speckling method based on wavelet transformation and bilateral filter is proposed for medical ultrasound images. The bilateral filter not only has better speckle reduction performances but also can preserve image edge details. To improve efficiency and to shorten running time, a fast bilateral filter based on FFT [18] is adopted in this paper.

Therefore, advantages of the wavelet de-noising method and the fast bilateral filter will be combined in this paper. The main idea of our proposed method is as follows: On the basis of the traditional wavelet de-noising method, an improved wavelet threshold function and a new shrinkage algorithm are suggested according to the statistical properties of speckle noise in wavelet domain medical ultrasound images. This new method can effectively suppress the speckle noise in high-pass component. Speckle noise in the low-pass approximation component of medical ultrasound images in the wavelet domain is filtered by the fast bilateral filter. The proposed method not only guarantees speckle reduction but also can greatly shorten running time.

## 2. The model of medical ultrasound image

Assuming that insonification and the resulting echo signal absorption have sufficiently obtained appropriate dynamic compensation from the ultrasound imaging system, the final ultrasonic envelope signal obtained consists of two parts: the reflected signal of the human body, which is a useful signal, and the noise itself, which is made up of two components, multiplicative noise and additive noise. Multiplicative noise is associated with the principle of ultrasonic signal imaging, which results from a random scattering phenomenon in imaging cell resolution. Additive noise can be considered system noise, such as sensor noise [17]. The ultrasonic envelope signal $f^{pre}(i,j)$ is modeled as follows:

$$f^{pre}(i,j) = g^{pre}(i,j)n^{pre}(i,j) + w^{pre}(i,j), \tag{1}$$

where $(i, j) \in Z^2$ is the two-dimensional spatial coordinates, and the superscript *pre* is the preliminary signal obtained by system. $g^{pre}(i,j)$ and $f^{pre}(i,j)$ denote the original signal and the observed signal, respectively. $n^{pre}(i,j)$ and $w^{pre}(i,j)$ represent the multiplicative and additive components of the noise, respectively, where the $n^{pre}(i,j)$ is the main component of noise.

The effect of additive noise $w^{pre}(i,j)$ on the qualities of the medical ultrasound images is less significant than the multiplicative noise $n^{pre}(i,j)$, and in order to simplify the model (1), the additive noise $w^{pre}(i,j)$ is generally omitted and the following model is obtained

$$f^{pre}(i,j) = g^{pre}(i,j)n^{pre}(i,j), \quad (i,j) \in Z^2. \tag{2}$$

Due to the limited dynamic range of commercial display monitors, ultrasound imaging systems compress the envelope signal with logarithmic transformation to fit in the display range [14]. Logarithmic amplification converts the model (2) into the classical additive noise model as follows:

$$\log(f^{pre}(i,j)) = \log(g^{pre}(i,j)) + \log(n^{pre}(i,j)), \tag{3}$$

where the signal $\log(f^{pre}(i,j))$ is the common medical ultrasonic image.

Since wavelet transformation is a linear transformation, the following model is obtained after two-dimensional discrete wavelet transformation for model (3):

$$W^j_{l,k}(f) = W^j_{l,k}(g) + W^j_{l,k}(n), \tag{4}$$

where $j = 1, 2, \ldots, J, l, k \in Z^2$. $W^j_{l,k}(f)$, $W^j_{l,k}(g)$ and $W^j_{l,k}(n)$ represent the wavelet coefficients of noisy images, noise-free images and speckle noise, respectively. The superscript $j$ represents the decomposition layers of wavelet transformation, and the subscripts $(l, k)$ are wavelet domain coordinates. $J$ denotes the largest decomposition layers. In order to facilitate the representation, we can rewrite (4) as:

$$F^j_{l,k} = G^j_{l,k} + N^j_{l,k}. \tag{5}$$

Since the Bayesian maximum a posteriori estimation will be used to develop a new wavelet shrinkage algorithm in this paper, and since the prior probability of noise-free signal and speckle noise is the premise of using the Bayesian maximum a posteriori estimation, we consider that the wavelet coefficients of noise-free signal will obey the generalized Laplacian distribution [4], and the wavelet coefficients of speckle noise will obey zero mean Gaussian distribution.

The wavelet coefficients of noise-free signal $G^j_{l,k}$ obey the generalized Laplacian distribution, and the probability distribution is:

$$p_G(g) = \frac{\nu}{2s\Gamma(1/\nu)} \exp\left(-\left|\frac{g}{s}\right|^{\nu}\right), \quad s, \nu > 0, \tag{6}$$

where $\Gamma(a) = \int_0^\infty x^{a-1}\exp(-x)\,dx$ represents Gamma function, $s$ is scale parameter, and $\nu$ is shape parameter. When $\nu$ is selected as 1, formula (6) becomes the Laplacian distribution, which is a special model of generalized Laplacian distribution.

The wavelet coefficients of speckle noise $N^j_{l,k}$ obey zero mean Gaussian distribution

$$p_N(n) = \frac{1}{\sqrt{2\pi}\sigma_N} \exp\left(-\frac{n^2}{2\sigma_N^2}\right), \tag{7}$$

where $\sigma_N$ denotes the standard deviation of noise in wavelet domain.

## 3. An improved de-speckling method based on wavelet shrinkage algorithm and fast bilateral filter

On the basis of the traditional wavelet de-noising method, three contributions are made and an improved de-speckling method based on the wavelet shrinkage algorithm with fast bilateral filter is proposed.

1) According to the statistical properties of medical ultrasound images in the wavelet domain, an improved threshold function based on the universal threshold function is proposed, which is more consistent with the de-noising of medical ultrasound images.
2) According to the statistical models of noise and signal in the wavelet domain, Bayesian maximum a posteriori estimation is applied to design a new shrinkage algorithm.
3) The speckle noise in the low-pass approximation component is filtered by the fast bilateral filter to ensure that this de-noising algorithm has a stronger ability to suppress speckle noise in the low-pass approximation component.

### 3.1. An improved wavelet threshold function

Donoho and Johnstone [14] designed a universal wavelet threshold function, i.e. $T = \sigma_N\sqrt{2\log M}$, where $M$ is the number of the wavelet coefficients in the corresponding wavelet domain. However, when $M$ becomes very large, the bigger threshold could smooth out some useful information, and thus this threshold function is ineffective on the noise removal in medical ultrasonic images. The following improvement is designed in order to obtain the desirable effect:

$$T_j = a_j\sigma_N\sqrt{2\ \log M} \tag{8}$$

where $j(=1, 2, \ldots, J)$ are the decomposition layers of wavelet transformation, $J$ denotes the largest decomposition layers. In this paper, $a_j$ represents the adaptive parameter of $j$ layer, and is determined experimentally. After wavelet decomposition, the wavelet coefficients in different decomposition layers have different distribution, and thus the selection of $a_j$ should be based on the $j$, and $a_j$ is selected as $1/\ln(j+1)$. But this choice of $a_j$ is not the optimal one, and if $a_j$ is selected appropriately, the proposed method will reflect more advantageously.

### 3.2. An improved wavelet shrinkage algorithm

The wavelet coefficients of noise-free signal $G^j_{l,k}$ and speckle noise $N^j_{l,k}$ obey the generalized Laplasse distribution and Gaussian distribution, respectively. In order to simplify the calculation, $\nu$ is selected as 1, so Eq. (6) can be simplified as follows:

$$p_G(g) = \frac{1}{2s}\exp\left(-\frac{|g|}{s}\right), \quad s > 0. \tag{9}$$

Bayesian maximum a posteriori estimation is used to obtain estimation of signal in the wavelet domain. In the process of calculating posterior probability, the following Bayesian equation is used:

$$p_{G|F}(g|f) = \frac{1}{p_F(f)}p_{F|G}(f|g)\cdot p_G(g) = \frac{1}{p_F(f)}p_N(f-g)\cdot p_G(g) \tag{10}$$

with Eqs. (7) and (9), Eq. (10) can be restated as:

$$p_{G|F}(g|f) = \frac{1}{p_F(f)}\cdot\frac{1}{2\sqrt{2\pi}s\sigma_N}\times\exp\left(\frac{2\sigma_N^2|g| - s(f-g)^2}{2s\sigma_N^2}\right) \tag{11}$$

In order to get the maximum a posteriori probability, the first-order derivative equal to zero of $\ln(p_{G|F}(g\,|f))$ with respect to $g$ leads to Eq. (12):

$$\hat{g} = \mathrm{sign}(f)\cdot\max\left(|f| - \frac{\sigma_N^2}{s}, 0\right) \tag{12}$$

where $\hat{g}$ is the estimation of $g$, $f$ is assumed in phase with noise-free signal $g$.

Finally, according to the above equation, a new wavelet shrinkage algorithm based on the improved threshold function and shrinkage algorithm is proposed:

$$\hat{g} = \begin{cases} 0, & f \le T_j \\ \mathrm{sign}(f)\cdot\max\left(|f| - \frac{\sigma_N^2}{s}, 0\right), & f > T_j \end{cases} \tag{13}$$

### 3.3. The bilateral filter

The main idea of wavelet de-noising method is to retain the wavelet coefficients of the low-pass component (LL), while wavelet coefficients of high-pass component (LH, HL, HH) are shrunk with the wavelet threshold function. However, only using the wavelet transformation de-noising algorithm to suppress speckle noise in medical ultrasonic images does not produce optimal results. In the experiment, it can be found that the wavelet coefficients in the low-pass component still contain some speckle noise. In order to effectively eliminate speckle noise in the low-pass component, the bilateral filter is selected to filter the speckle noise.

#### 3.3.1. Traditional bilateral filter

The bilateral filter output at each pixel is a weighted average of its neighbors. The weight is assigned to each neighbor, which decreases with both the distance of the image plane (the spatial domain $S$) and the distance on the intensity axis (the range domain $R$). When a Gaussian $G_\sigma$ is used as a decreasing function, the structure of traditional bilateral filter is given as the following [18]:

$$I^b_p = \frac{1}{W^b_p}\sum_{q\in S}G_{\sigma_s}(||p-q||)G_{\sigma_r}(|I_p - I_q|)I_q, \tag{14}$$

where $I$ is the input image and $I^b$ is the result of the bilateral filter. $W^b_p = \sum_{q\in S}G_{\sigma_s}(||p-q||)G_{\sigma_r}(|I_p - I_q|)$ normalizes the sum of the weights. The parameter $\sigma_s$ defines the size of the spatial neighborhood to filter a pixel, and $\sigma_r$ controls the weight with its adjacent pixels according to the intensity difference.

#### 3.3.2. The fast bilateral filter

The bilateral filter has been proven effective to filter speckle noise in the low-pass component, but it has a high computational cost, and is difficult to be applied in real-time systems. Especially for the medical ultrasound images, the image resolutions are usually very large, which limit the application of the bilateral filter to a great extent, and thus the fast bilateral filter is proposed. The fast bilateral filter is also known as higher-dimensional bilateral filter. In the fast bilateral filter, the gray levels of pixels are combined to form a 3D space from a 2-D image domain. Thus, the original complex nonlinear component has been shifted to a linear convolution of a three-dimensional Gaussian kernel function and a three-dimensional image function. Using this higher dimensional space, the convolution computation can be down-sampled without significant impact on the resulting accuracy. Then, fast Fourier transformation is applied to calculate linear convolution. This approximation technique enables a speed-up of several orders of magnitude and controls the induced error.

The structure of fast bilateral filter is as follows:

$$BI(x,y) = \frac{IY(x,y)}{EY(x,y)} = \frac{interp(G\otimes IX, (x/s_s), (y/s_s), (I(x,y)/s_r))}{interp(G\otimes EX, (x/s_s), (y/s_s), (I(x,y)/s_r))} \tag{15}$$

where $IX(x,y,z) = \begin{cases} z, z = I(x,y) \\ 0, z \ne I(x,y) \end{cases}$ represents the three-dimensional image matrix, $EX(x,y,z) = \begin{cases} 1, z = I(x,y) \\ 0, z \ne I(x,y) \end{cases}$ represents

the three-dimensional weight matrix, and *interp* is the interpolation function. $G$ is a Gaussian kernel function after linearization. $s_s$ and $s_r$ denote the sample rate of spatial domain and range domain, respectively.

As can be observed from Eq. (15), the fast bilateral filter is expressed as a linear convolution of the increment dimensional matrix and an increment dimensional kernel function. The 3D matrix *IX* and *EX* are filtered by 3D Gaussian filter, respectively. Then, the linear interpolation is used to revert two filtering results to a two-dimensional matrix *IY* and *EY*. Finally, *EY* is divided by *BI* to obtain a restored image *BI*. In 3D space, sampling, convolution and interpolation realize the acceleration for several orders of magnitude.

### 3.4. Parameter estimation

The standard deviation of speckle noise $\sigma_n$ is obtained from the wavelet coefficients of highest frequency in the wavelet domain ($F_{i,k}^{HH^1}$) [14]:

$$\hat{\sigma}_N = \frac{median(|F_{i,k}^{HH^1}|)}{0.6745} \tag{16}$$

where $\hat{\sigma}_N$ is the estimation of $\sigma_N$, this equation had been proven by Donoho in soft-threshold. With Eq. (5), it can be obtained as follows:

$$\sigma_{F,j}^2 = \sigma_{G,j}^2 + \sigma_N^2. \tag{17}$$

Because $G_{l,k}^j$ and $N_{l,k}^j$ were modeled as zero mean models (Eqs. (6) and (7)), the standard deviation of wavelet coefficients in $j$ layer $\sigma_{F,j}$ can be calculated by the standard deviation of wavelet coefficients $F_{l,k}^j$:

$$\hat{\sigma}_{F,j} = \sqrt{\frac{1}{N}\sum_{l,k=1}^{m,n}(F_{l,k}^j - mean)^2} = \sqrt{\frac{1}{N}\sum_{l,k=1}^{m,n}(F_{l,k}^j)^2} \tag{18}$$

where $N = m \times n$ is the total number of wavelet coefficients in corresponding wavelet domain, $m$ and $n$ are the rows and columns of wavelet coefficients in corresponding wavelet domain, respectively.

Based on Eqs. (16)–(18):

$$\hat{\sigma}_{G,j}^2 = \max(\hat{\sigma}_{F,j}^2 - \hat{\sigma}_N^2, 0) \tag{19}$$

In this paper, scale parameter $s$ in Eq. (9) can be estimated as the following equation, which has been proven in literature [4]:

$$s = [0.5(\sigma_{F,j}^2 - \sigma_N^2)]^{0.5} = \frac{\hat{\sigma}_{G,j}}{\sqrt{2}}. \tag{20}$$

### 3.5. The method steps

1) Ultrasonic envelope signal received by the ultrasonic imaging system is compressed with logarithmic transformation, and thus the multiplicative noise model is converted to an additive noise model. If the image is the common medical ultrasonic image, which has been processed with the logarithmic transformation, this step can be omitted.
2) The 2-D discrete wavelet transformation (DWT) is applied for the log-transformed image, and four frequency domains ($LL^1$, $LH^1$, $HL^1$ and $HH^1$) are obtained. To continue the process of wavelet decomposition for the low frequency domain $LL^1$, four frequency domains ($LL^2$, $LH^2$, $HL^2$ and $HH^2$) are obtained. This step is repeated until the maximum decomposition layer $J$ is reached.
3) According to Eq. (15), the fast bilateral filter is used to filter the low-pass component of the last layer ($LL^J$).
4) Based on Eq. (13), the new threshold shrinkage algorithm is used to process the wavelet coefficients of the high-pass components in each layer ($LH^j$, $HL^j$ and $HH^j$, $j = 1, 2, \ldots, J$). The standard deviation of speckle noise, image and no-noise signals are obtained by Eqs. (16), (18) and (19), respectively. The threshold of each layer is obtained from Eq. (8), and parameter $s$ is determined by Eq. (20).
5) Inverse wavelet transformation is used to obtain the de-noised medical ultrasonic images.

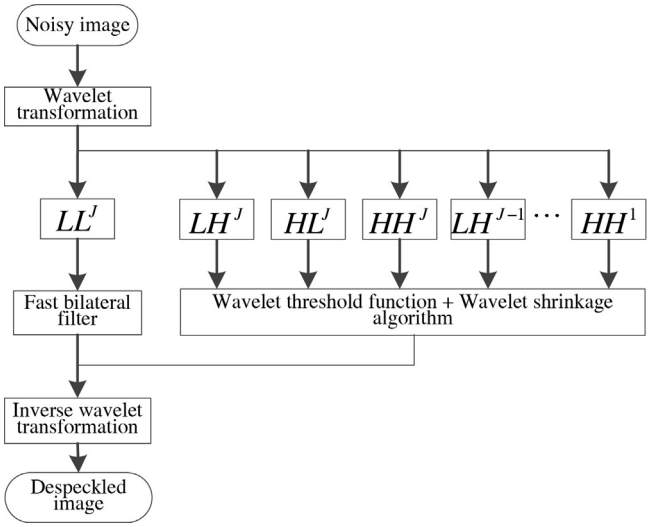


**Fig. 1.** The schematic diagram of the proposed algorithm.

In addition, the exponential transformation can be used to process the de-noised medical ultrasonic images to get the de-noised ultrasonic envelope signal.

The schematic diagram of the proposed algorithm is as shown in Fig. 1.

## 4. The experimental study of the proposed de-speckling method

In order to objectively evaluate the de-noising method proposed in this paper, the peak signal-to-noise ratio (PSNR), the structural similarity (SSIM), FoM (Pratt's Figure of Merit) and the running time are chosen as evaluation criteria of the experiments. The PSNR is given by:

$$PSNR(X, \hat{X}) = 10 \lg\left(\frac{255^2}{MSE}\right) \tag{21}$$

where $\hat{X}$ is the estimation of signal $X$, and *MSE* is:

$$MSE = \frac{1}{MN}\sum_{i=1}^{M}\sum_{j=1}^{N}(X_{i,j} - \hat{X}_{i,j})^2 \tag{22}$$

where $M$ and $N$ represent the length and width of the two-dimensional signal $X$, respectively.

SSIM is an image quality metrics to measure the structure similarity between two images, and its definition is as follows [19]:

$$SSIM(X, \hat{X}) = \frac{(2\mu_X\mu_{\hat{X}} + c_1)(2\sigma_{X,\hat{X}} + c_2)}{(\mu_X^2 + \mu_{\hat{X}}^2 + c_1)(\sigma_X^2 + \sigma_{\hat{X}}^2 + c_2)} \tag{23}$$

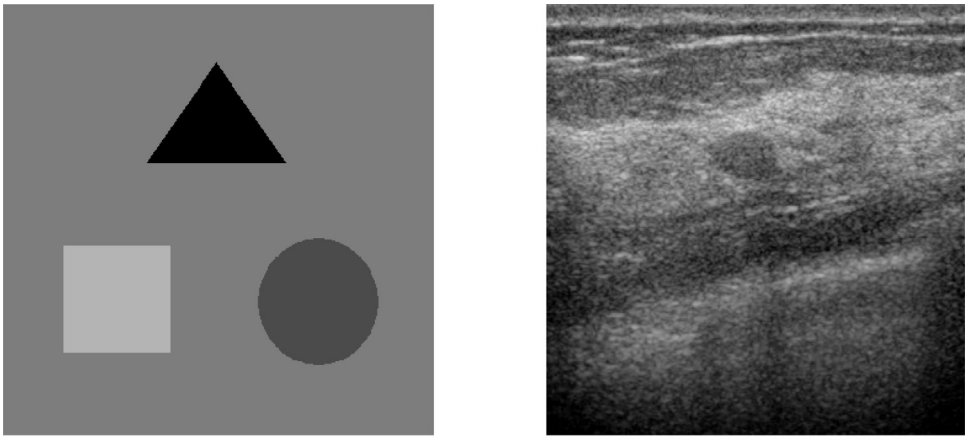


**Fig. 2.** Images used for experiments.

where $\mu_X$, $\mu_{\hat{X}}$, $\sigma_X^2$ and $\sigma_{\hat{X}}^2$ denote the mean and variance of reference image and their estimation, respectively. $\sigma_{X,\hat{X}}$ represents the covariance of $X$ and $\hat{X}$. $c_1$ and $c_2$ are constants. When $c_1$ and $c_2$ are selected as positive, the value range of SSIM is [0 1], and 1 is the best result, which means that the two pictures have the same structure.

FoM can be used to objectively evaluate the performance of edge detectors, and its definition is [20]:

$$FoM(X,\hat{X}) = \frac{1}{\max(N_X, N_{\hat{X}})}\sum_{i=1}^{N_X}\frac{1}{1+\alpha d_i^2} \tag{24}$$

where $N_X$ and $N_{\hat{X}}$ represent the ideal and the actual detected edge pixel number, respectively. $\alpha$ is a constant (usually $\alpha = 1/9$), and $d_i$ represents the distance of the $i$th edge pixel to the nearest ideal edge pixel. The value range of FoM is [0 1], and 1 is the best result, which means that the detected image edge is consistent with the ideal image edge. In the experiment, Canny detection algorithm is used in detecting edge pixel (the standard deviation of Gaussian filter $\sigma = 3$).

The images in Fig. 2 are used for experiments. Fig. 2(a) is designed for simulation ($350 \times 350$ pixels), and Fig. 2(b) is a clinical medical ultrasound image with lesions (a breast ultrasound image of women, $340 \times 350$ pixels).

In this paper, the experiments are divided into two branches: one is the speckle noise simulation experiment, and the other is the medical ultrasound image experiment. The experimental schematic diagram is given in Fig. 3.

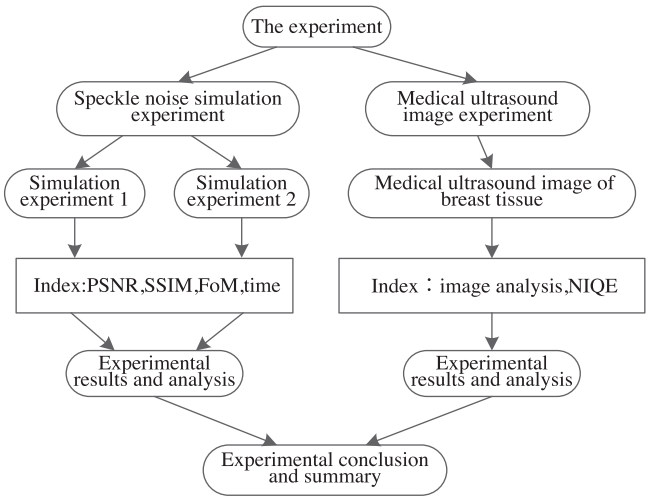


**Fig. 3.** The experimental schematic diagram.

### 4.1. Experiments for simulated ultrasound images

In order to quantitatively estimate the de-noising effect of the method proposed in this paper, two speckle noise simulation experiments are conducted. The low-pass filter is used for the Gaussian random field of complex domain, and its amplitude is simulated as speckle noise. The simulated image is shown in Fig. 2(a). The parameters of the Gaussian random field [21] are: the mean $\mu = 0$, and the rational quadratic covariance function $r_\theta(l) = (1 + (1/\theta_1^2))^{-\theta_2}$, where two non-negative parameters are selected as $\theta_1 = 1$ and $\theta_2 = 1.2$, respectively.

#### 4.1.1. Simulation experiment 1

Since our method achieved acceleration through approximation, we have to measure the numerical accuracy by comparing the outputs of our technique with traditional bilateral filter. Fig. 2(a) is selected as noise-free image; the result is shown in Fig. 4 and Table 1, where the Gaussian parameters (space and range) of two filters are chosen as $\sigma_s = 2.5$ and $\sigma_r = 0.045$, respectively.

#### 4.1.2. Simulation experiment 2

In order to evaluate the accuracy and performance of the proposed de-noising method in this experiment, the results obtained with the proposed de-noising method are compared with six other kinds of de-noising methods (SRBF [8], DPAD [9], Andria [15], OBNLM [5], SAR-BM3-D [16] and Wavelet-Soft Shrinkage [14]). Parameters of the six filters in this experiment are listed in Table 2. To obtain better filtered results, these parameters are proposed by both the cited papers and medical experts. Fig. 2(a) is chosen as noise-free image, and the simulation experimental results are shown in Fig. 5 and Table 3, where all the algorithms ran at Matlab R2010a.

**Table 1**
Performance comparison of simulation experiment 1.

| | PSNR | SSIM | FoM | Time(s) |
|---|---|---|---|---|
| Noisy image | 24.7141 | 0.4593 | 0.1763 | – |
| Traditional bilateral filter | 27.8670 | 0.6823 | 0.2432 | 7.7813 |
| Fast bilateral filter | 27.0225 | 0.8497 | 0.2367 | 1.1079 |

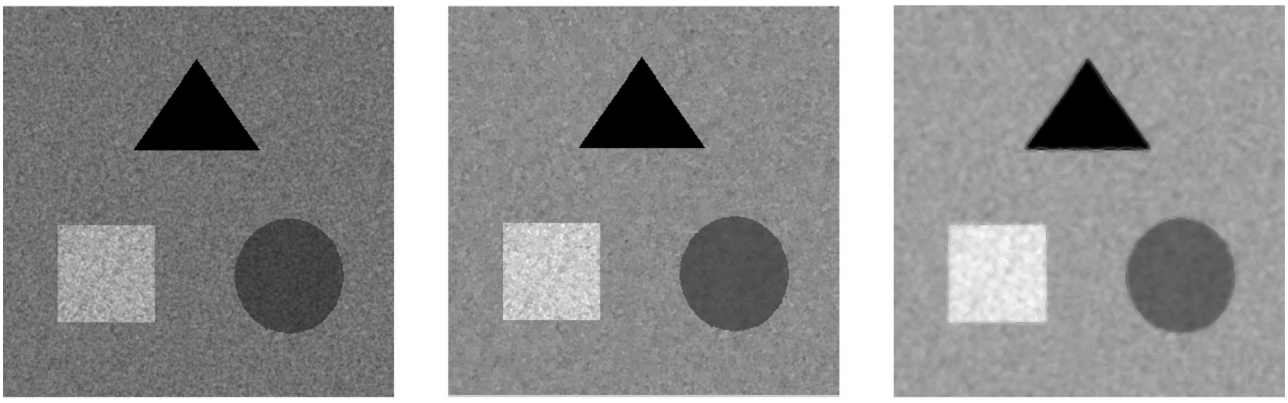


**Fig. 4.** De-noised results of simulation experiment 1.

**Table 2**
The parameters of filters for experiments.

| Method | Reference | Date | Category | Experiment parameters |
|---|---|---|---|---|
| SRBF | [8] | 2010 | Local adaptive | Window size $5 \times 5$ |
| DPAD | [9] | 2006 | Anisotropic diffusion | Window size $5 \times 5$, time step $\Delta t = 0.2$, iteration times $t = 100$ |
| Andria | [15] | 2012 | Multi-scale | Window size $5 \times 5$, decomposition level $J = 1$ |
| OBNLM | [5] | 2009 | Nonlocal means | Window size $7 \times 7$, search area size $15 \times 15$, smoothing parameter $h = 0.6$ |
| SAR-BM3-D | [16] | 2012 | Hybrid | Window size $8 \times 8$, search area size $39 \times 39$, decomposition level $J = 3$ |
| Wavelet-Soft Shrinkage | [14] | 1995 | Multi-scale | Window size $3 \times 3$, wavelet = 'coif1', decomposition level $J = 4$ |

### 4.2. Experiments for medical ultrasound images

The experiments for clinical ultrasound breast images are presented in this section. The clinical ultrasound breast images are acquired using Vivid 7 ultrasound unit (GE Medical System) with an operating frequency range of 2.3–10.0 MHz. The ultrasound breast images are recorded as displayed on a Vivid 7 monitor after logarithmic compression. The image resolution is $350 \times 340$ pixels with 256 gray levels, approximately representing $36 \times 35$ mm. There are 200 asymptomatic and 200 symptomatic ultrasound breast images obtained for the clinical experiment, which are provided by ultrasound medical experts. The result is shown in Fig. 6 and Table 4.

### 4.3. Interpretations of experimental results

#### 4.3.1. A simulation experiment

Fig. 4 and Table 1 show de-noised results of the traditional bilateral filter and the fast bilateral filter with the same settings. According to the evaluation criteria, the fast bilateral filter not only has good de-noising effect but also greatly reduces the running time compared with the traditional bilateral filter.

In our experiment, some new strong speckle reducing filters, which belong to different categories, are applied to the simulated images, and the filtered results for the simulated image of these filters are shown in Fig. 5, respectively. It can be observed that the Frost filter (Fig. 5(b)) reduces more speckles while its output result appears blurry. For the DPAD filter (Fig. 5(c)), it obtains a more obvious speckle reducing effect, but introduces small artifacts to some extent. Among multi-scale filters, Andria (Fig. 5(d)) and Wavelet-Soft Shrinkage (Fig. 5(g)) do not produce a satisfactory speckle reducing effect. The OBNLM filter (Fig. 5(e)) and the SAR-BM3-D filter (Fig. 5(f)) achieve above-average results with regard to speckle reduction. Especially, the SAR-BM3-D filter exhibits the impressive de-speckling ability. Although the OBNLM filter has strong speckle reduction performance, it introduces some textual man-made artifact. The proposed de-noising method based on wavelet transformation and fast bilateral filter, which also belongs to the category of the hybrid filter, has a strong speckle noise reducing ability, and at the same time it keeps the major edge information.

**Table 3**
Performance comparison of simulation experiment 2.

| De-noising method | PSNR | SSIM | FoM | Time(s) |
|---|---|---|---|---|
| Noisy image | 24.7141 | 0.4593 | 0.1763 | – |
| SRBF | 26.1535 | 0.9022 | 0.1574 | 10.2188 |
| DPAD | 27.8729 | **0.9316** | 0.2265 | 12.7031 |
| Andria | 25.0185 | 0.5113 | 0.1662 | 0.6094 |
| OBNLM | 27.0275 | 0.9039 | **0.3512** | 30.0082 |
| SAR-BM3-D | 27.4333 | 0.9236 | 0.2192 | 130.8637 |
| Wavelet-Soft Shrinkage | 26.2004 | 0.7459 | 0.1808 | 1.7188 |
| Wavelet + bilateral | 32.7396 | 0.9032 | 0.2929 | 9.6406 |
| Wavelet + fast bilateral | **33.4424** | 0.9072 | 0.3175 | 1.1224 |

The bold values represent the best value in the corresponding index, which can help reader to know which de-noising method performs better in this index.

**Table 4**
NIQE of images in Fig. 6.

| De-noising methods | NIQE |
|---|---|
| Noisy image | 5.7915 |
| SRBF | 7.3026 |
| DPAD | 4.5330 |
| Andria | 7.3836 |
| OBNLM | 6.6960 |
| SAR-BM3-D | 8.2565 |
| Wavelet-Soft Shrinkage | 7.3725 |
| Wavelet + bilateral | 9.5018 |
| Wavelet + fast bilateral | **10.1890** |

The bold values represent the best value in the corresponding index, which can help reader to know which de-noising method performs better in this index.

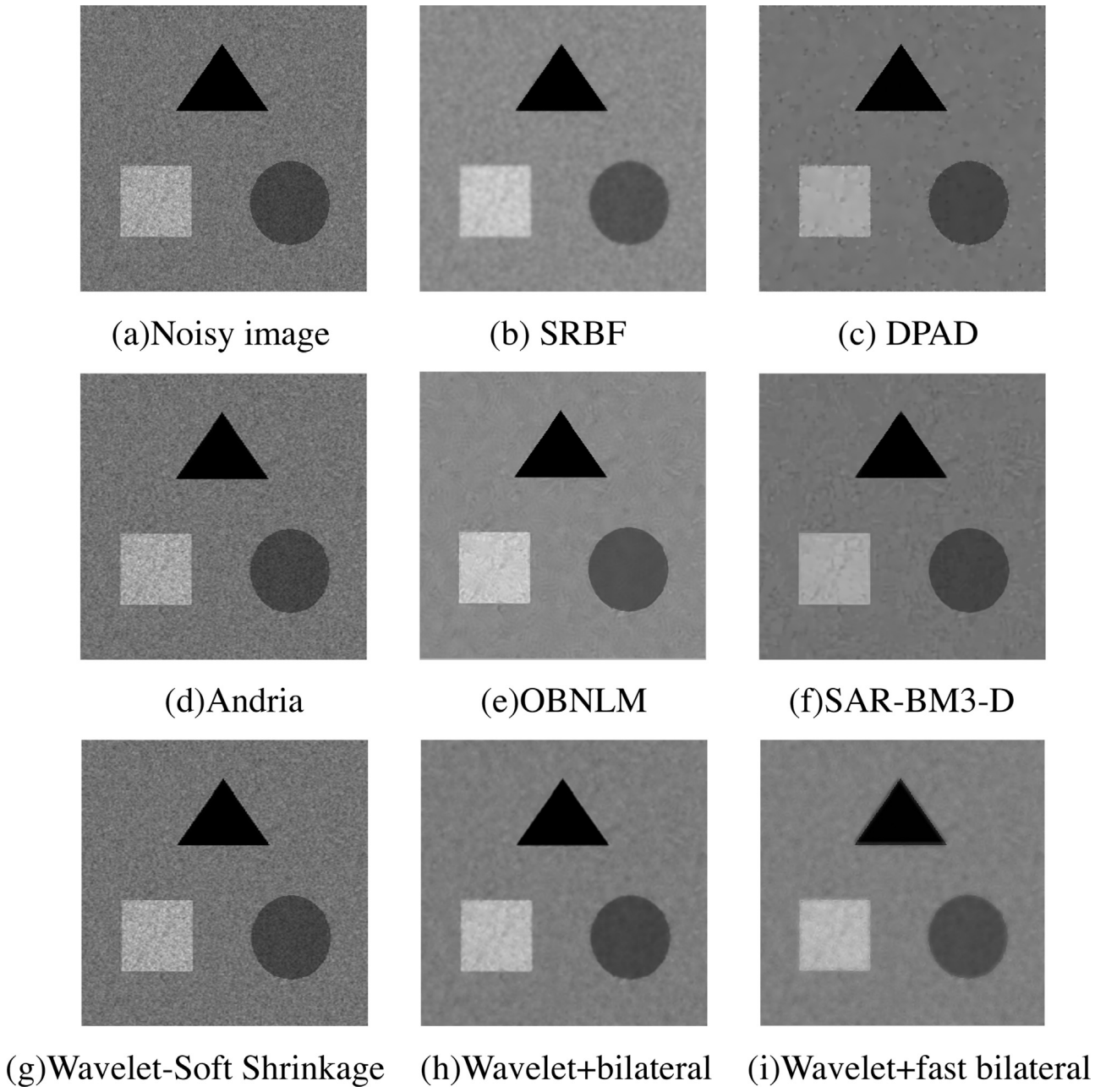


**Fig. 5.** De-noised results of simulation experiment 2.

In order to objectively evaluate the above de-noising methods, the comparison of evaluation criteria is shown in Table 3. The PSNR values in Table 3 measure the ability of speckle reduction. From Table 3, the SRBF filter does not provide a satisfactory value. The DPAD filter outperforms some other filters, which means that the DPAD filter has a strong de-speckle ability. Among the multi-scale filters, the Andria filter gets the lowest value and the Wavelet-Soft Shrinkage also does not provide a satisfactory value. Thus from the results, it can be observed that multi-scale filters have poor performance. For the OBNLM filter and the SAR-BM3-D filter, they perform better than SRBF filter and multi-scale filters. It also can be observed from the results that the proposed method, which is improved based on wavelet de-noising method, not only garners the better result than Wavelet-Soft Shrinkage, but also performs better than the others.

Table 3 shows the SSIM values of the filtered simulated images, and SSIM quantifies the structure similarity of the two images. The larger the SSIM (the largest SSIM being, 1) value of the two comparing images, the more similar they are in structure. By comparing these filters, it can be observed that the multi-scale filters (Andria and Wavelet-Soft Shrinkage) have the lowest SSIM value, which means that the output images filtered with the Andria filter and the Wavelet-Soft Shrinkage filter have less similar structure. The DPAD filter obtains better performance and has the highest SSIM value. It can be readily observed that the SAR-BM3-D filter outperforms other filters with higher SSIM values in speckle noise simulated images, which means the output images filtered with the SAR-BM3-D filter have more similar structure. The other filters (the SRBF filter, the OBNLM filter and the proposed filters) all obtain favorable results.

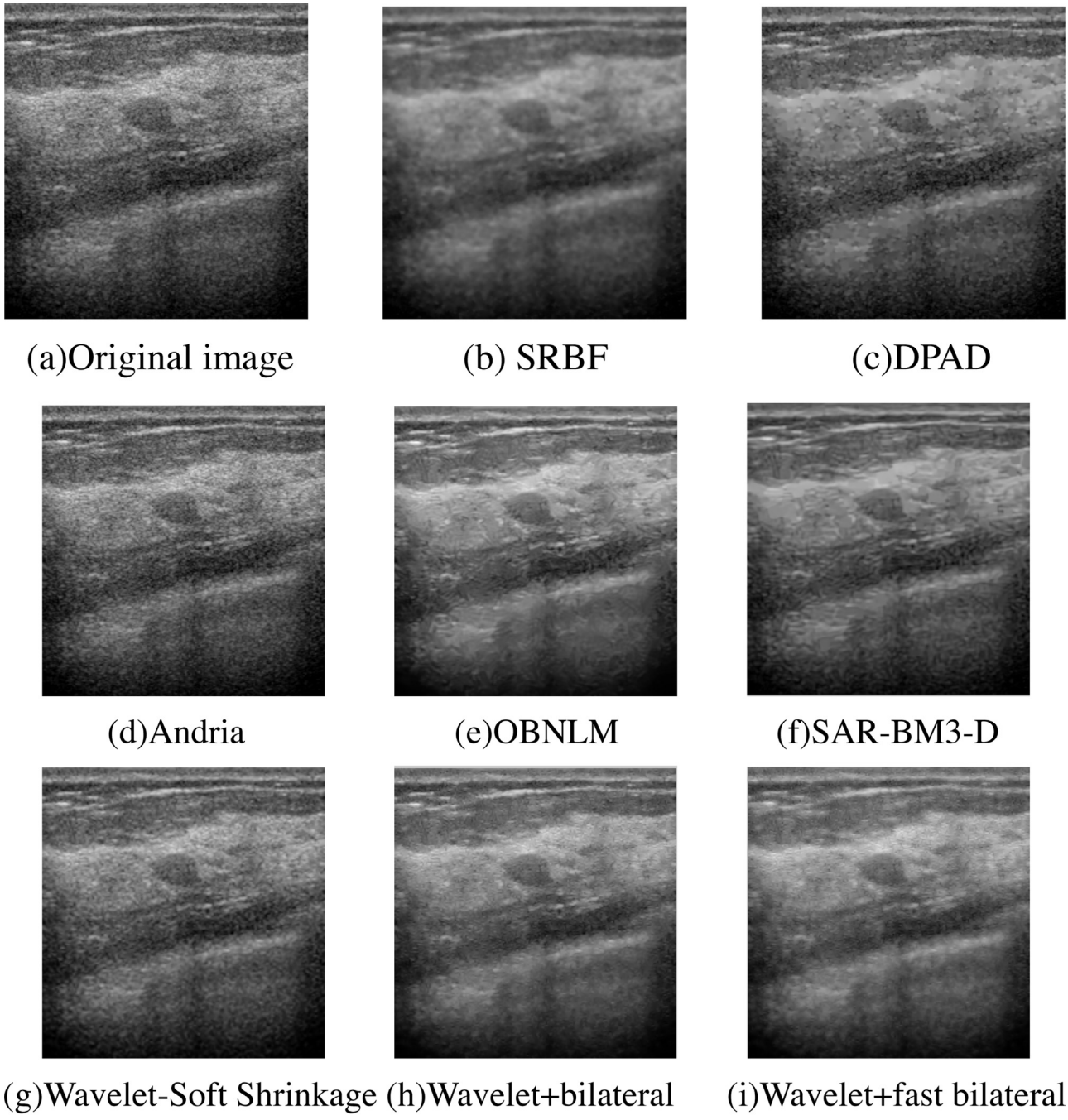


**Fig. 6.** De-noised results of clinical ultrasound images.

Table 3 also shows the result of FoM values, which measure similarity of the image edge between the noise-free image and the filtered output image. It is observed that the OBNLM filter and the proposed filter outperform other filters by comparing the similarity of the ideal image edge. The other filters do not have comparable performances.

For medical ultrasound images, the de-noising processing time is also a factor to be considered, and a filter which needs too much time to process is difficult to be applied in real-time systems. Table 3 also shows the running time results. It can be observed that the OBNLM filter and the SAR-BM3-D take too much time. Thus they cannot be suitable for medical ultrasound images. The SRBF, DPAD, and wavelet + bilateral filters' running time is not too long. But the medical ultrasound image resolutions are usually very large, so these filters will take too much time processing the medical ultrasound images. In Table 3, only the multi-scale filters (Andria and Wavelet-Soft Shrinkage) and the Wavelet + fast bilateral filter can improve speed.

From the above analysis, according to standards in medical ultrasound images, it can be seen that the proposed method (Wavelet + fast bilateral) performs better than others. Although the SAR-BM3-D and OBNLM filters have good speckle reduction, they are not time effective and although the multi-scale filters take less time, they do not have satisfactory speckle reduction performance.

Comparing the SRBF, DPAD and Wavelet + bilateral filters, and by considering the speckle reduction and running time, it is obvious that the proposed method outperforms other filters. The proposed method has the maximum value of PSNR, and this means it has better de-noising effect for the simulated image. With other image quality metrics, the proposed method has good structural similarity and quality of edge detection. What is more, the proposed method has greatly improved the running time due to the combination with the fast bilateral filter.

#### 4.3.2. Experiments for medical ultrasound images

A group of representative filtered ultrasound breast images are shown in Fig. 6. It can be observed that the SRBF filter (Fig. 6(b)) has a better speckle reduction performance but the edges appear somewhat blurred. In Fig. 6(c), the DPAD filter shows a strong speckle reduction but introduces small artifacts. Among the multi-scale filters, the Wavelet-Soft Shrinkage filter (Fig. 6(g)) can suppress some speckle noise, while the Andria filter (Fig. 6(d)) only reduces a little speckle. Both the OBNLM (Fig. 6(e)) and SAR-BM3-D filters (Fig. 6(f)) have very fine speckle suppression performance, but considering the time factor, the two methods are not desirable. Only the proposed method has the strong speckle reduction while retaining the edge information.

Because of the fact that the ultrasound images without noise do not exist, PSNR and other image quality metrics cannot be effectively used in the clinical ultrasound images experiment. So, another image quality metric is introduced to evaluate the quality of de-noised images, which is NIQE (no-reference image quality assessment). From Table 4, it is shown that the proposed method has the highest NIQE value, which means the proposed method has the best speckle reduction effect in comparison. Additionally, the DPAD filter performs poorly in NIQE metric due to the reason that some obvious artifacts (as in massive mosaics) appear in the filtered image (Fig. 6(c)).

It can be seen from above that although the SRBF filter has low algorithm complexity, it tends to blur the details of the image, and the speckle noise suppression effects are not satisfactory. The DPAD filter has strong de-noising ability, but the results may create an overly smooth phenomenon and introduce some man-made artifacts. Among the multi-scale filters (Andria and Wavelet-Soft Shrinkage), although the speckle reduction effect is not satisfactory, they do not need too much time, and thus the wavelet de-noising method combined in the proposed method. From the experiments, the OBNLM filter has the ideal speckle noise suppression performance, but it is not easy to meet the real-time requirement of medical ultrasonic imaging systems due to the disadvantage of high algorithm complexity. In fact, the target of the hybrid filters is to combine the advantages of different filters. As for the SAR-BM3-D filter, because of the combination of the non-local means filter, it is not time effective. The proposed method is the combination of the wavelet de-noising method with fast bilateral filter. Thus it not only ensures effective de-noising but also greatly reduces running time.

## 5. Conclusions

In this paper, a de-speckling method for medical ultrasound images based on wavelet transformation with fast bilateral filter is proposed to solve the problem of speckle noise in medical ultrasound images. Three main achievements are attained:

(1) Based on the general wavelet threshold function, a new threshold function is designed according to the statistical characteristics in the wavelet domain of medical ultrasound images. The new threshold function is closely related to the wavelet decomposition layers.
(2) The noise-free signal and speckle noise in the wavelet domain are modeled as generalized Laplace distribution model and Gaussian model, respectively. The Bayesian maximum a posteriori estimation method is used to obtain a new shrinkage algorithm.
(3) Because speckle noise still exists in the low frequency component after wavelet decomposition, the fast bilateral filter is introduced to suppress speckle noise in the low frequency component.

The experiments are divided into two branches. The simulation experiment, by comparing the PSNR, SSIM and FoM metrics, demonstrated that the proposed method greatly improves the efficiency of de-noising, and has good speckle reduction. An experiment with clinical images of women's breast ultrasounds concluded that ultrasound images without noise do not exist when no-reference image quality metrics (NIQE) are applied. Although the NIQE is not specifically designed for ultrasound images originally, the result of evaluating ultrasound breast images can be proven to be useful (see Table 4).

In conclusion, this study has shown the results of our current research. From the results of simulation experiments and medical ultrasound image experiments, the proposed method can not only suppress speckle noise well but also greatly improves the efficiency of de-noising.

## Acknowledgments

The authors thank the anonymous reviewers for their valuable comments and suggestions that will help improve the manuscript. The authors would also thank the people who provided the MATLAB code or executable file, especially Jiawen Chen for the fast bilateral filter. The work is partially supported by National Natural Science Foundation of China (60974042).

## References

[1] K. Abd-Elmoniem, A. Youssef, Y. Kadah, Real-time speckle reduction and coherence enhancement in ultrasound imaging via nonlinear anisotropic diffusion, IEEE Trans. Biomed. Eng. 49 (9) (2002) 997–1014.
[2] M.F. Insana, R.F. Wagner, B.S. Garra, D.G. Brown, T.H. Shawker, Analysis of ultrasound image texture via generalized Rician statistics, Opt. Eng. 25 (6) (1986) 743–748.
[3] P.M. Shankar, A general statistical model for ultrasonic backscattering from tissues, IEEE Trans. Ultrason. Ferroelectr. Freq. Control 47 (1) (2000) 727–736.
[4] N. Gupta, M.N.S. Swamy, E. Plotkin, Despeckling of medical ultrasound images using data and rate adaptive lossy compression, IEEE Trans. Med. Imaging 24 (6) (2005) 743–754, http://dx.doi.org/10.1109/TMI.2005.847401.
[5] P. Coupé, P. Hellier, C. Kervrann, et al., Nonlocal means-based speckle filtering for ultrasound images, IEEE Trans. Image Process. 18 (10) (2009) 2221–2229, http://dx.doi.org/10.1109/TIP.2009.2024064.
[6] J. Lee, Digital image enhancement and noise filtering by use of local statistics, IEEE Trans. Pattern Anal. Mach. Intell. 2 (2) (1980) 165–168.
[7] V. Frost, J. Stiles, K. Shanmugan, et al., A model for radar images and its application to adaptive digital filtering of multiplicative noise, IEEE Trans. Pattern Anal. Mach. Intell. 4 (2) (1982) 157–166.
[8] S. Balocco, C. Gatta, O. Pujol, et al., SRBF: speckle reducing bilateral filtering, Ultrasound Med. Biol. 36 (8) (2010) 1353–1363.
[9] S. Aja-Fernández, C. Alberola-López, On the estimation of the coefficient of variation for anisotropic diffusion speckle filtering, IEEE Trans. Image Process. 15 (9) (2006) 2694–2701, http://dx.doi.org/10.1109/TIP.2006.877360.
[10] J. Yu, J. Tan, Y. Wang, Ultrasound speckle reduction by a SUSAN-controlled anisotropic diffusion method, Pattern Recognit. 43 (2010) 3083–3092, http://dx.doi.org/10.1016/j.patcog.2010.04.006.
[11] K. Krissian, C. Westin, R. Kikinis, et al., Oriented speckle reducing anisotropic diffusion, IEEE Trans. Image Process. 16 (5) (2007) 1412–1424, http://dx.doi.org/10.1109/TIP.2007.891803.
[12] C. Deledalle, L. Denis, F. Tupin, Iterative weighted maximum likelihood denoising with probabilistic patch based weights, IEEE Trans. Image Process. 18 (12) (2009) 2661–2672, http://dx.doi.org/10.1109/TIP.2009.2029593.

[13] Y. Guo, Y. Wang, T. Hou, Speckle filtering of ultrasonic images using a modified non local-based algorithm, Biomed. Signal Process. Control 6 (2011) 129–138, http://dx.doi.org/10.1016/j.bspc.2010.10.004.
[14] D.L. Donoho, I.M. Johnstone, Ideal spatial adaptation via wavelet shrinkage, Biometrika 81 (1994) 425–455.
[15] G. Andria, F. Attivissimo, G. Cavone, et al., Linear filtering of 2-D wavelet coefficients for denoising ultrasound medical images, Measurement 45 (2012) 1792–1800.
[16] S. Parrilli, M. Poderico, C.V. Angelino, et al., A nonlocal SAR image denoising algorithm based on LLMMSE wavelet shrinkage, IEEE Trans. Geosci. Remote Sens. 50 (2) (2012) 606–616, http://dx.doi.org/10.1109/TGRS.2011.2161586.
[17] E.K. Abd, A. Youssef, Y. Kadah, Real-time speckle reduction and coherence enhancement in ultrasound imaging via nonlinear anisotropic diffusion, IEEE Trans. Biomed. Eng. 49 (9) (2002) 997–1014, http://dx.doi.org/10.1109/TBME.2002.802051.
[18] S. Paris, F. Durand, A fast approximation of the bilateral filter using a signal processing approach, Int. J. Comput. Vis. 81 (2006) 24–52.
[19] Z. Wang, A.C. Bovik, H.R. Sheikh, Image quality assessment: from error visibility to structural similarity, IEEE Trans. Image Process. 13 (4) (2004) 600–612, http://dx.doi.org/10.1109/TIP.2003.819861.
[20] S. Finn, M. Glavin, E. Jones, Echocardiographic speckle reduction comparison, IEEE Trans. Ultrason. Ferroelectr. Freq. Control 58 (1) (2011) 82–101, http://dx.doi.org/10.1109/TUFFc.2011.1776.
[21] B. Kozintsev, B. Kedem, Generation of "similar" images from a given discrete image, J. Comput. Graph. Stat. 9 (2) (2000) 286–302.